Hindawi
Neural Plasticity
Volume 2020, Article ID 8869526, 13 pages
https://doi.org/10.1155/2020/8869526

Research Article

Acute Effects of Two Different Species of Amyloid-β on Oscillatory Activity and Synaptic Plasticity in the Commissural CA3-CA1 Circuit of the Hippocampus

Cécile Gauthier-Umaña,[1] **Jonathan Muñoz-Cabrera**,[2] **Mario Valderrama**,[3] **Alejandro Múnera**,[2] **and Mauricio O. Nava-Mesa**[1]

[1]*Neuroscience Research Group (NEUROS), Escuela de Medicina y Ciencias de la Salud, Universidad del Rosario, Bogotá, Colombia*
[2]*Behavioral Neurophysiology Laboratory, Physiological Sciences Department, School of Medicine, Universidad Nacional de Colombia, Bogotá, Colombia*
[3]*Deparment of Biomedical Engineering, Universidad de los Andes, Bogotá, Colombia*

Correspondence should be addressed to Mauricio O. Nava-Mesa; monavam@usal.es

Received 23 April 2020; Revised 4 December 2020; Accepted 8 December 2020; Published 19 December 2020

Academic Editor: Javier M rquez Ruiz

Recent evidence indicates that soluble amyloid-β (Aβ) species induce imbalances in excitatory and inhibitory transmission, resulting in neural network functional impairment and cognitive deficits during early stages of Alzheimer's disease (AD). To evaluate the *in vivo* effects of two soluble Aβ species (A$\beta_{25\text{-}35}$ and A$\beta_{1\text{-}40}$) on commissural CA3-to-CA1 (cCA3-to-CA1) synaptic transmission and plasticity, and CA1 oscillatory activity, we used acute intrahippocampal microinjections in adult anaesthetized male Wistar rats. Soluble Aβ microinjection increased cCA3-to-CA1 synaptic variability without significant changes in synaptic efficiency. High-frequency CA3 stimulation was rendered inefficient by soluble Aβ intrahippocampal injection to induce long-term potentiation and to enhance synaptic variability in CA1, contrasting with what was observed in vehicle-injected subjects. Although soluble Aβ microinjection significantly increased the relative power of γ-band and ripple oscillations and significantly shifted the average vector of θ-to-γ phase-amplitude coupling (PAC) in CA1, it prevented θ-to-γ PAC shift induced by high-frequency CA3 stimulation, opposite to what was observed in vehicle-injected animals. These results provide further evidence that soluble Aβ species induce synaptic dysfunction causing abnormal synaptic variability, impaired long-term plasticity, and deviant oscillatory activity, leading to network activity derailment in the hippocampus.

1. Introduction

Alzheimer's disease (AD), the most common type of dementia and progressive neurodegenerative disorder worldwide, is characterized by selective neuronal loss, and two histopathological features in *postmortem* tissue are extracellular amyloid plaques composed of amyloid beta peptide (Aβ) and intracellular neurofibrillary tangles composed of hyperphosphorylated tau protein [1]. Recent evidence indicates that soluble forms of Aβ induce glutamatergic, cholinergic, and GABAergic imbalance, resulting in functional impairment of neural networks during early AD stages [2–5]. In fact, Aβ-induced synaptic dysfunction precedes selective neuronal degeneration and may explain memory impairment during early AD stages and mild cognitive impairment, a prodromal stage of AD [6, 7]. Although therapies based on modulation of GABAergic neurotransmission have been proposed for AD [8], current symptomatic therapies include cholinesterase inhibitors and NMDA antagonists only [9]. New Aβ-targeted immunotherapies have been tested in several clinical trials but without a clear clinical benefit [10]; therefore, no course-modifying treatment has been

developed to date because of a lack of understanding of the fundamental mechanisms underlying AD, as well as the physiological role of amyloid peptides.

Senile plaques in AD patients and animal models consist of $A\beta_{1\text{-}40}$ and $A\beta_{1\text{-}42}$ ($A\beta_{1\text{-}42}$ mainly in the core of early plaques and $A\beta_{1\text{-}40}$ in vascular amyloid deposits) [11, 12]. It has been suggested that short Aβ fragments, such as $A\beta_{25\text{-}35}$, constitute the biologically active forms of Aβ and are thus responsible for the neurotoxic properties of $A\beta_{1\text{-}40}$ and $A\beta_{1\text{-}42}$ [13]. $A\beta_{25\text{-}35}$ may be expressed in AD brains [14–16] possibly from enzymatic cleavage of $A\beta_{1\text{-}40}$ [15, 16]. Several studies indicate similar effects in the brain of either short or long forms of Aβ [13–15]. However, $A\beta_{25\text{-}35}$ produces more acute toxic effects than $A\beta_{1\text{-}42}$ because of its higher solubility [17], and it also has different effects on synaptic plasticity and intracellular pathophysiological mechanisms compared with $A\beta_{1\text{-}40}$ and $A\beta_{1\text{-}42}$ [18–20].

The hippocampus and entorhinal cortex are peculiarly susceptible to deleterious Aβ effects during early AD stages [21]. Hippocampal plasticity, necessary for learning and memory processes, is tuned by θ activity, which depends on acetylcholine release from the medial septum [2]. Moreover, the septum and hippocampus are reciprocally interconnected and functionally coupled through GABAergic and glutamatergic connections to form the septohippocampal system [2, 22]. Each of these neurotransmitters contributes to hippocampal rhythmicity [23]. Moreover, θ and γ activities are associated through inhibitory synapses between GABAergic parvalbumin interneurons and pyramidal neurons [24]. Such oscillatory activity, including phase-to-amplitude coupling of θ and γ activity, is necessary for adequately encoding and storing information in the cortex and hippocampus [25–27]. *In vivo* studies have shown the relevance of the CA3-CA1 synapse in associative learning and memory processing [28, 29] and its implications in AD through animal models [30]. In a very recent study, the electrophysiological activity of the CA3-CA1 region in humans was correlated with memory tasks (i.e., delayed match-to-sample) and it resembles synaptic hippocampal responses observed in rodents in the same areas [31]. Therefore, studies based on animal models may provide physiological information that could be applied in specific regions of clinical relevance in the human brain.

There are tight correlations among long-term potentiation (LTP) mechanisms, θ-γ oscillations, and hippocampal-dependent memories [32–34]. Event-locked oscillatory activity in hippocampal formation and hippocampus-related structures is necessary for learning and long-term memory processes, as well as for declarative and spatial memory functions, which are impaired in early stages of AD [3, 34, 35]. Accumulating evidence indicates that Aβ affects θ, δ, and γ bands in different preclinical models of AD [3, 36]. Similarly, EEG recordings in AD patients show pathological changes of network oscillations in a wide range of frequencies (i.e., α/θ ratio, γ coherence, θ and δ synchronization) [37, 38]. Studies using an animal model of AD (transgenic CRND8 mice) indicate that alterations in θ-γ cross-frequency coupling might be used as an early biomarker of AD [39]. In another study, acute LTP impairment by $A\beta_{1\text{-}42}$ was related to alterations in oscillatory activity in θ-γ coupling at perforant path-dentate gyrus synapses [40]. Various studies have reported that changes in the spectral power of brain oscillations are related to LTP induction and expression [32, 33, 41, 42] and have shown a relationship between changes in single-synapse and network oscillation activity. Therefore, Aβ-induced LTP impairment might be associated with oscillatory activity changes in brain structures affected during initial stages of AD.

Several aggregated Aβ forms and configurations may explain variable effects during AD progression. Considering the huge differences between experimental models (*in vivo vs. in vitro*), time of exposure to Aβ (acute *vs.* chronic), and differences in Aβ aggregation states (monomeric, oligomeric, and fibrillary), the reported Aβ effects on neuronal activity have been divergent in terms of excitability, active and passive membrane properties, network activity, and neural plasticity [22, 43–47]. Despite the large number of studies, little is known about the effects of diverse soluble Aβ forms on oscillatory activity, excitability, or synaptic plasticity [47, 48]. The aim of the present study was, therefore, to evaluate $A\beta_{25\text{-}35}$ and $A\beta_{1\text{-}40}$ effects on hippocampal oscillations (power spectral density and phase-amplitude coupling) and basal transmission, variability, and long-term plasticity in cCA3-to-CA1 synapses. We found that LTP impairment induced by acute administration of soluble Aβ ($A\beta_{1\text{-}40}$ and $A\beta_{25\text{-}35}$) is associated with abnormal synaptic variability and increased power of γ-band and ripple network oscillations and derailed θ-to-γ phase-to-amplitude coupling in CA1. Such Aβ-induced disruption in synaptic plasticity and network activity may underlie abnormalities in information processing and memory encoding.

2. Material and Methods

2.1. Ethical Statement. All procedures performed on living animals were performed in conformance with Animal Research: Reporting *In Vivo* Experiments (ARRIVE) guidelines [49], following the Guide for the Care and Use of Laboratory Animals (8th edition, National Institutes of Health) and fulfilling the Colombian regulation (Law 84/1989 and Resolution 8430/1993). In addition, every experimental design and all procedures were approved by the Universidad del Rosario Ethics Committee.

2.2. Animals. Seventeen 16-20-week-old male Wistar rats, weighing 300 ± 30 g, were used as experimental subjects. Experimental animals were supplied by the Universidad Nacional de Colombia animal facilities. Animals were housed in a sound-attenuated room in polycarbonate cages, in groups of four, under controlled environmental conditions: $20 \pm 1^{\circ}$C temperature, $50 \pm 10\%$ relative humidity, and 12 h light/dark cycle (lights on from 07:00 to 19:00). Animals had food and water available *ad libitum*. Experiments were performed in the morning. Special care was taken to minimize animal suffering and to reduce the number of animals used.

Sample size was calculated according to the following formula [50]: $\text{sample size} = 2\text{SD}^2\left(Z^{\alpha/2} + Z^{\beta}\right)^2/d^2$, where $\text{SD} = 6.85$, $Z^{\alpha/2} = 1.96$ with $\alpha = 0.05$, $Z^{\beta} = 0.84$ with $\beta = 0.2$.

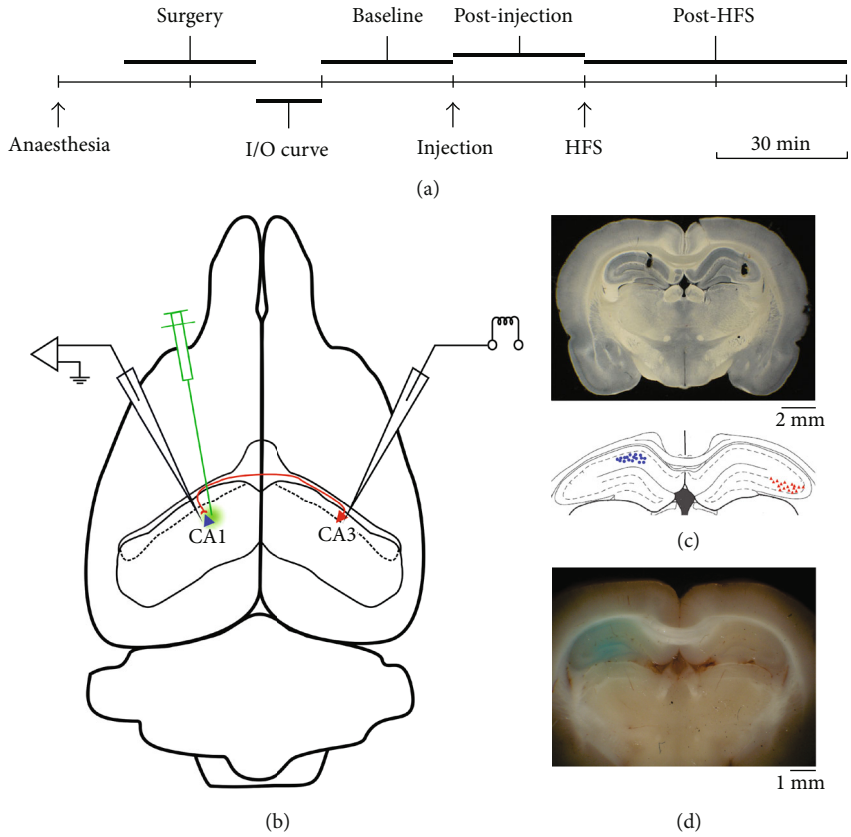

Figure 1: Experimental timeline and preparation. (a) Timeline indicating the experimental procedures during a recording session. (b) Diagram of a rat brain illustrating microelectrode cannula (for local field potential recording and microinjection in left CA1) and stimulating electrode (in right CA3) locations. (c) Panoramic photograph of an obliquely illuminated coronal brain slice containing representative electrolytic lesions made by passing current through recording (left) and stimulating (right) electrodes (upper panel), paired to a corresponding coronal diagram of the hippocampus (extracted and modified from the bregma: -3.6 mm diagram of Paxinos' rat brain atlas), summarizing recording (left, blue circles) and stimulating (right, red triangles) electrode placement in each experimental subject. (d) Panoramic photograph of a brain block containing methylene blue-coloured left hippocampus, attesting adequate diffusion of the injected solution.

Statistical power = 80%, and $d = 14$. The minimum sample number per group was 5.

2.3. Experimental Design and Timeline. Animals were randomly assigned to any of three groups: (1) control group (n =6), receiving vehicle microinjection; (2) A$\beta_{25\text{-}35}$ group ($n = 6$), receiving A$\beta_{25\text{-}35}$ peptide microinjection; and (3) A$\beta_{1\text{-}40}$ group ($n = 5$), receiving A$\beta_{1\text{-}40}$ peptide microinjection.

In brief, each experiment proceeded as follows: (1) under general anaesthesia, recording and stimulation electrodes were stereotactically inserted in CA1 and contralateral CA3; (2) once stable responses were obtained, the input/output relationship was established; (3) 30 min baseline recording was done to characterize basal synaptic efficiency; (4) the designed solution was microinjected in CA1; (5) the microinjected solution's effect on synaptic transmission was characterized by recording synaptic responses for 30 min after microinjection; (6) high-frequency tetanic stimulation was done to induce long-term plasticity; and (7) the effect of high-frequency stimulation (HFS) on synaptic efficiency was characterized by recording synaptic responses for 60 min after HFS (Figure 1(a)).

2.4. Surgery. Under general anaesthesia induced with 1.5 g/kg of 25% urethane (Sigma-Aldrich, St. Louis, USA) and 10 mg/kg of xylazine (Rompun®, Bayer, Leverkusen, Germany) (intraperitoneal injection), the subject was placed in a rat stereotaxic frame (SR-6R, Narishige Inc., Tokyo, Japan). Nociceptive responses (tail prick and paw withdrawal reflex) were evaluated during the experiment. In case of slight motor response, an additional injection of urethane at 50% of the initial dose was administered. The respiratory and cardiac rates were monitored during the whole experiment, and a heating blanket was used to avoid hypothermia. Because we were interested in evaluating Aβ effects on NMDA-dependent synaptic plasticity, we chose urethane as the anaesthetic agent, taking into account that it has been reported to have no significant effects on NMDA-type glutamate receptors when given in intermediate doses [51, 52]; however, anaesthetic doses of urethane depress or even abolish 7-12 Hz atropine-resistant theta activity [53], but left 4-7 Hz atropine-sensitive theta oscillations unaltered. Longitudinal fronto-occipital incision, followed by connective and muscle tissue dissection, was used to expose the skull. Two holes were drilled in parietal bones: one for inserting a

recording electrode aimed at left CA1 (stereotaxic coordinates from the bregma: AP = −3.8 mm, L = 2.5 mm, left) and one for inserting a stimulating electrode aimed at right CA3 (stereotaxic coordinates from the bregma: AP = −3.8 mm, L = 3.7 mm, right) [54]. In order to reduce variability between subjects, we always use the same electrode configuration. The dura mater was cut and removed through the holes in order to allow electrode insertion (Figure 1(b)).

2.5. In Vivo Extracellular Electrophysiology. A microelectrode cannula (a 5 MΩ impedance enamel-coated wire attached to a 25-G needle), for local field potential (LFP) recording and microinjection, was inserted 2.5 mm from the pial surface, through the skull hole for left CA1 (vide supra for stereotaxic coordinates), using a hydraulic micromanipulator (SM-25C, Narishige Inc., Tokyo, Japan). A stimulating concentric bipolar electrode was lowered 3.5 mm from the pial surface, through the skull hole for right CA3 (vide supra for stereotaxic coordinates), using a micromanipulator (SM-25A, Narishige Inc., Tokyo, Japan). A silver electrode was placed in neck musculature as a reference.

CA1 field activity was magnified (100x) using an AC-coupled preamplifier (NEX-1, Biomedical Engineering, New York, USA). The preamplified signal was then band-pass filtered (0.1 Hz and 10 kHz cut-off frequencies) and further amplified at 20x (yielding 2000x total gain). This conditioned signal was digitized using an analogue-to-digital converter (DigiData 1200, Molecular Devices, San José, USA) with 10 kHz sampling frequency and stored for offline analysis using commercial (Clampfit, Molecular Devices, San José, USA) and purpose-designed software.

CA3 was stimulated by applying 100 μs monophasic square pulses, delivered at 0.33 Hz frequency, using a stimulus isolation unit (Isolator-11, Molecular Devices, San José, USA), controlled by a pulse generator (9514 Plus, Quantum Composers, Bozeman, USA). Stimulus intensity (100-400 μA) was adjusted so as to obtain stable and reliable CA1 field excitatory postsynaptic potentials (fEPSP). The depth of the stimulating and recording electrodes from the pial surface was finely adjusted so as to obtain short latency fEPSP, with a waveform characteristic of CA1 stratum pyramidale.

Once a stable CA1 fEPSP was achieved, threshold stimulus intensity was established by decreasing the intensity to one-half the previous one until the fEPSP failure rate was equal to or higher than 50% (characteristically 50 to 200 μA). Stimulus intensity was then successively doubled until fEPSP response saturation was attained (characteristically 4 to 8 times the threshold intensity). Then, the stimulus intensity required to obtain ~50% of maximal response (I_{50}) was selected to evaluate short- and long-term plasticity from then on. Basal synaptic activity was characterized by recording CA3 stimulation-evoked fEPSP in CA1 (I_{50} intensity, 100 μs duration, and 0.1 Hz frequency) for 30 min. Intrahippocampal microinjection effect on basal synaptic activity was characterized by recording such fEPSP for 30 min after microinjection. Long-term potentiation at cCA3-to-CA1 synapses was induced by delivering six trains (1 s length, 100 Hz frequency) at 60 s intertrain intervals (HFS). HFS effect on cCA3-to-CA1 synaptic efficiency was studied by recording left CA1 response to right CA3 stimulation (I_{50} intensity, 100 μs duration, and 0.1 Hz frequency) for 60 min. Deep anaesthetic level was maintained throughout the whole recording session using supplementary anaesthetic doses (about every 4 hours) to attain stable and reliable activity in CA1 [55].

Once the recording session ended, a terminal dose of anaesthesia (urethane 2 g/kg and xylazine 10 mg/kg, intraperitoneal) was given and the location of stimulating and recording electrode tips was marked by passing continuous current through them delivered by a precision current source (Midgard, Stoelting, Wood Dale, USA). The subject's brain was removed and submerged in 4% paraformaldehyde for 3 days; then, 100 μm thick coronal slices encompassing stimulating and recording sites were obtained using a vibratome (1000 Plus, Vibratome, Bannockburn, USA). The electrodes' position and diffusion trace of microinjection coloured solution were documented by examining the slices with a stereoscope (SZX16, Olympus, Tokyo, Japan) and taking digital photographs (Cybershot DSCW7, Sony, Tokyo, Japan) under oblique back-illumination (Figure 1(c)).

2.6. Preparation of Vehicle and Aβ Peptide Solutions. Among many soluble Aβ species, A$\beta_{25\text{-}35}$ and A$\beta_{1\text{-}40}$ (Sigma-Aldrich, St. Louis, USA) were chosen for the present work on the basis of their aggregation kinetics, neurotoxicity, and pathogenicity. On the one hand, postmortem examination of AD patients' brains yielded that A$\beta_{1\text{-}40}$ accounts for approximately 90% of total Aβ peptide in senile plaques [56]. On the other hand, A$\beta_{25\text{-}35}$ aggregates more rapidly and displays more neurotoxicity than A$\beta_{1\text{-}40}$ [13, 57]. A$\beta_{25\text{–}35}$ and A$\beta_{1\text{-}40}$ peptides were prepared as previously described [22, 43, 45]. Briefly, peptides were dissolved in 0.9% normal saline solution with 0.5% methylene blue to 1.5 mM concentration and stored at -20°C. Aliquots were defrosted and incubated at 37°C for 24 h before experiments [58, 59]. The vehicle solution was therefore 0.9% normal saline with 0.5% methylene blue. Methylene blue was used to attest adequate diffusion in the hippocampal CA1 region of either vehicle or Aβ peptides (Figure 1(d)).

2.7. Intrahippocampal Microinjection. Once a baseline recording was obtained, a Hamilton syringe connected through 12-G tubing was used to inject 2 μL of the designed solution (either vehicle, A$\beta_{25\text{-}35}$, or A$\beta_{1\text{-}40}$) at a 1 μL/min rate through the microelectrode cannula inserted in the left hippocampal CA1 region. A$\beta_{25\text{-}35}$ and A$\beta_{1\text{-}40}$ dose (3 nM) and total injection volume (2 μL) were chosen according to previous reports [60–63]. Stimulation and recording were restarted three minutes after microinjection in order to allow diffusion and prevent leakage of injected solution.

2.8. Data Analysis. Electrophysiological data analyses were planned to characterize the effects of both microinjected solutions on basal cCA3-to-CA1 synaptic responses, cCA3-to-CA1 long-term plasticity, and CA1 oscillatory activity. To do so, recordings were divided into 5 min windows around stimulation events and analysed in time, frequency,

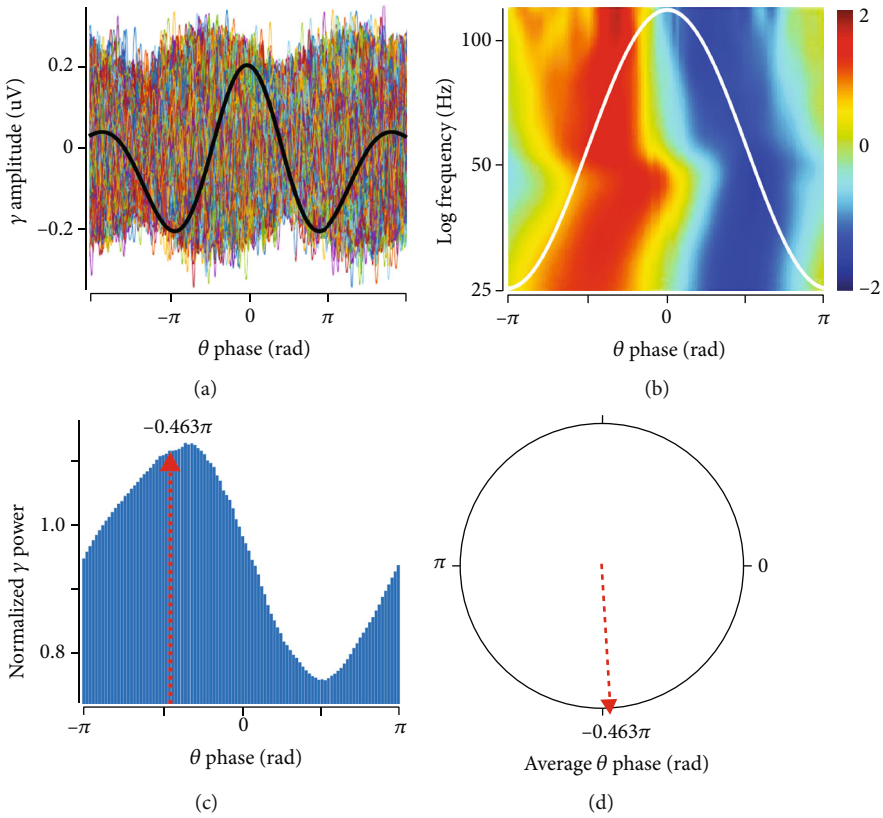

FIGURE 2: θ-to-γ phase-amplitude coupling (PAC) analysis process. (a) Filtered LFP in θ (black trace) and γ bands (coloured traces) are represented; θ trace is the average of n theta cycles, aligned around their maximum amplitude (downscaled to fit γ amplitude); each θ cycle-concurrent γ activity is presented in superposition using the abovementioned alignment. (b) Average normalized γ band scalogram (colour scale) relative to the θ phase (illustrated as a white trace). (c) Normalized γ band spectral power average as a function of the θ phase. (d) Average vector of (c) indicating dominant-phase θ-to-γ PAC.

and time-frequency domains. Time domain analysis was related to fEPSP first component slope measurement. Frequency domain analysis was focused on calculating relative power spectral density (rPSD) in δ (0.5-3.9 Hz), θ (4-7.9 Hz), α (8-11.9 Hz), β (12-24.9 Hz), γ (25-120 Hz), HFO_1 (121-250 Hz), and HFO_2 (250-500 Hz) bands, using Welch's method. Time-frequency domain analysis was done by building scalograms for each window, using the Morse wavelet decomposition [64, 65]; then, γ band scalogram averages were triggered by each θ cycle time window to determine phase-amplitude coupling (PAC) [66] (Figure 2). Detailed information about mathematical data processing, which was done using self-written scripts using MATLAB R2017a® (The MathWorks, Inc., Natick, Massachusetts, USA), can be found in Supplementary Materials (available here).

2.9. Statistics. According to data distribution normality, determined using the Shapiro-Wilk test, long-term plasticity and PSD data from experimental groups were compared using either one-way ANOVA or Kruskal-Wallis one-way analysis of variance by rank modules of SigmaPlot 12.0 (Systat Software, Inc., San José, California, USA). Variability of cCA3-to-CA1 synaptic responses from experimental groups was compared using Levene's test [67]. The resulting angle from the average PAC vector in the experimental groups was compared using the MATLAB toolbox for circular statistics [68].

3. Results

3.1. Aβ Did Not Alter Synaptic Efficiency but Induced Changes in Synaptic Variability. No significant difference was found between the experimental groups during baseline recording before ($H_{(2)} = 0.153$, $p = 0.797$, $n = 16$) or after intrahippocampal injection ($F_{(2,13)} = 1.541$, $p = 0.251$, $n = 16$: Figure 3(a)). However, fEPSP slope variability significantly changed after intrahippocampal injection ($F_{(2,461)} = 64.898$, $p < 0.001$, $n = 16$); *post hoc* analysis showed that $A\beta_{1\text{-}40}$ microinjection significantly increased cCA3-to-CA1 synaptic variability more than the other treatments (control *vs.* $A\beta_{25\text{-}35}$: $F_{(1,317)} = 0.004$, $p = 0.951$, $n = 11$; control *vs.* $A\beta_{1\text{-}40}$: $F_{(1,287)} = 71.932$, $p < 0.001$, $n = 10$; and $A\beta_{1\text{-}40}$ *vs.* $A\beta_{25\text{-}35}$: $F_{(1,318)} = 86.351$, $p < 0.001$, $n = 11$). Variability progressively increased in control and $A\beta_{25\text{-}35}$ groups after both injection (control: $F_{(1,606)} = 19.232$, $p < 0.001$, $n = 5$; $A\beta_{25\text{-}35}$: $F_{(1,636)} = 23.761$, $p < 0.0001$, $n = 6$) and HFS (control: $F_{(1,438)} = 63.522$, $p < 0.0001$, $n = 5$; $A\beta_{25\text{-}35}$: $F_{(1,438)} = 49.588$, $p < 0.0001$, $n = 6$). By contrast, even though variability in the $A\beta_{1\text{-}40}$ group increased substantially after being injected

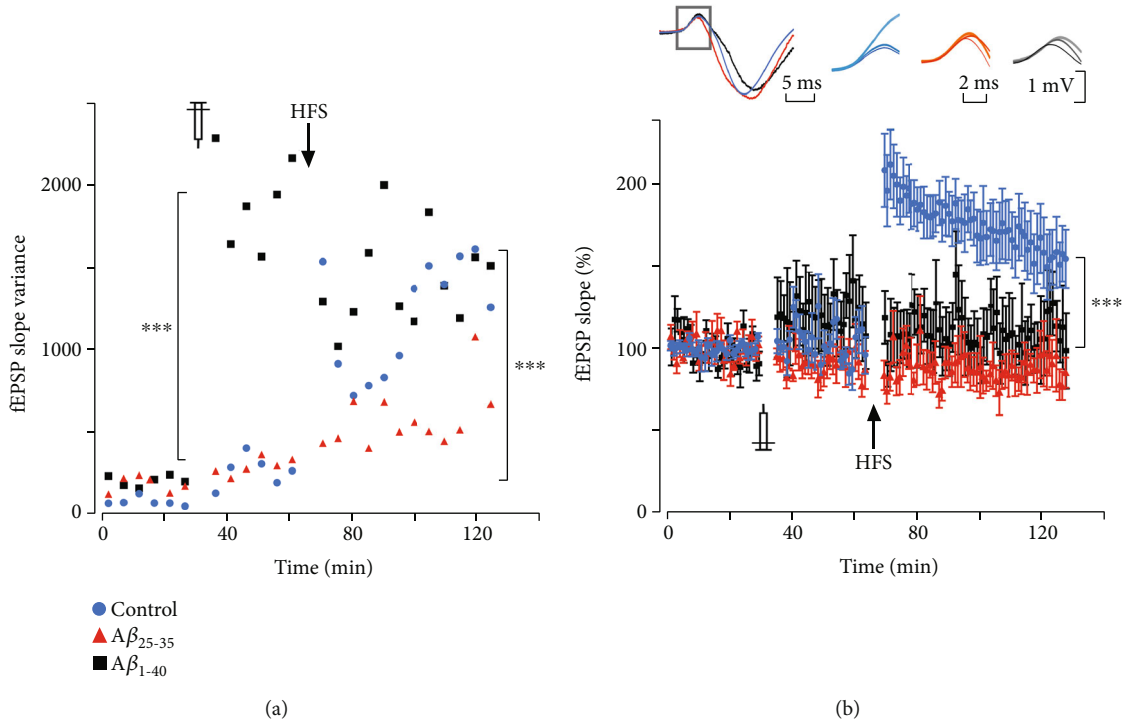

Figure 3: Intrahippocampal Aβ injections altered synaptic variability and impaired LTP in cCA3-to-CA1 synapse. Temporal evolution of slope variability (a) and magnitude (b) of cCA3 stimulation-evoked EPSP in CA1 recorded along three consecutive experimental stages, from left to right: (1) 30 min before peptide injection (baseline), (2) 30 min after intrahippocampal injection, and (3) after HFS (six 1 s, 100 Hz trains, delivered every 60 s). EPSP variability increased after intrahippocampal injection, being significantly higher in the A$\beta_{1\text{-}40}$ group. HFS induced significant LTP in vehicle-injected subjects but not in Aβ-injected ones. In (a), each dot represents 5 min variance of slope; in (b), each dot illustrates 2 min mean ± standard error of the mean (SEM). Inset in (b): left—representative whole CA1 fEPSP average from each experimental group evoked by I_{50} stimuli delivered in contralateral CA3 (the region representing the monosynaptic component is outlined by a gray rectangular box); right—three sets of average traces (10 trials per average) of the monosynaptic component of cCA3 stimulation-evoked CA1 field potential obtained during baseline (thin line, dark colour), after intrahippocampal injection (intermediate line, intermediate colour), and after HFS (thick line, light colour) for each experimental group (control, blue; A$\beta_{25\text{-}35}$, red; and A$\beta_{1\text{-}40}$, black). ***Significant differences between groups ($p < 0.001$). Data from each experimental group were normalized respecting the average value obtained during the last 15 min of baseline.

($F_{(1,606)} = 299.08$, $p < 0.0001$, $n = 5$), it did not change after HFS ($F_{(1,438)} = 0.63$, $p = 0.428$, $n = 5$).

3.2. Aβ Impaired Long-Term Synaptic Plasticity. HFS induced significant fEPSP slope increase in vehicle-injected subjects (from 100 ± 0.91% to 198.8 ± 14%, $H_{(2)} = 9.5$, $p = 0.009$, $n = 5$). By contrast, both A$\beta_{25\text{-}35}$ and A$\beta_{1\text{-}40}$ impaired such HFS-induced fEPSP slope increase (A$\beta_{25\text{-}35}$: from 100 ± 1.29% to 89.45 ± 16%, $F_{(2,17)} = 0.504$, $p = 0.614$, $n = 6$; A$\beta_{1\text{-}40}$: from 100 ± 1.84% to 113.5 ± 25%, $F_{(2,17)} = 0.938$, $p = 0.418$, $n = 5$; Figure 3(b)). Indeed, fEPSP slope change after HFS was significantly different between groups ($F_{(2,15)} = 17.741$, $p < 0.001$, $n = 16$); *post hoc* analysis (Tukey's test) showed that vehicle-injected subjects displayed fEPSP slope increase significantly greater than A$\beta_{25\text{-}35}$- and A$\beta_{1\text{-}40}$-injected ones (control *vs.* A$\beta_{25\text{-}35}$: $Q = 8.146$, $p < 0.001$, $n = 11$; control *vs.* A$\beta_{1\text{-}40}$: $Q = 6.083$, $p = 0.002$, $n = 10$), while these later groups were not significantly different to each other ($Q = 1.792$, $p = 0.437$, $n = 11$). These results show that soluble Aβ microinjection impairs cCA3-to-CA1 long-term synaptic plasticity.

3.3. A$\beta_{25\text{-}35}$ Induced Increase in γ and HFO$_1$ Band Relative PSD. Intrahippocampal injection of A$\beta_{25\text{-}35}$ induced significant increases in relative PSD (Figure 4) in γ (Figure 4(a), left column, $F_{(2,11)} = 8.237$, $p = 0.007$, $n = 17$) and HFO$_1$ (Figure 4(b), left column, $H_{(2)} = 6.408$, $p = 0.029$, $n = 17$) bands, but not in other bands. Neither A$\beta_{1\text{-}40}$ nor vehicle injection induced significant changes in relative PSD in any band (Suppl. Table 1). In A$\beta_{25\text{-}35}$-injected subjects, HFS did not induce additional changes in γ (Figure 4(a), right column; 5 min: $F_{(2,11)} = 3.036$, $p = 0.089$; 30 min: $H_{(2)} = 1.96$, $p = 0.403$; and 60 min: $F_{(2,11)} = 1.502$, $p = 0.265$), HFO$_1$ (Figure 4(b), right column; 5 min: $F_{(2,11)} = 0.063$, $p = 0.940$; 30 min: $F_{(2,11)} = 0.224$, $p = 0.803$; and 60 min: $F_{(2,11)} = 0.341$, $p = 0.718$), or any other band. HFS did not induce significant changes in relative PSD in any band in vehicle- or A$\beta_{1\text{-}40}$-injected subjects (Suppl. Table 2). In summary, only A$\beta_{25\text{-}35}$, which is the more toxic soluble species of Aβ, induced increased energy contribution in gamma and HFO$_1$ bands, but HFS did not further modify such changes.

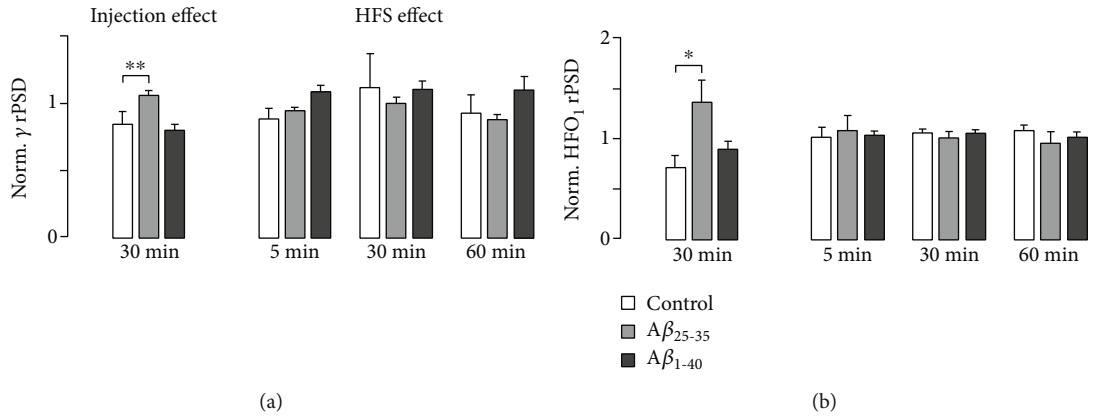

Figure 4: Peptide injection but not HFS increased rPSD in γ and HFO1 bands. Bar diagrams illustrating rPSD in γ (a) and HFO1 (b) bands. The left panel shows the effect of peptide or vehicle, 30 min after injection, normalized respecting baseline rPSD in the same bands. The right panel shows the effect of HFS normalized regarding rPSD calculated after injection in the same bands. Bars and whiskers represent each group's mean + SEM. *Significant difference respecting the control group during baseline ($p < 0.05$); **significant difference respecting each group after peptide injection ($p < 0.01$).

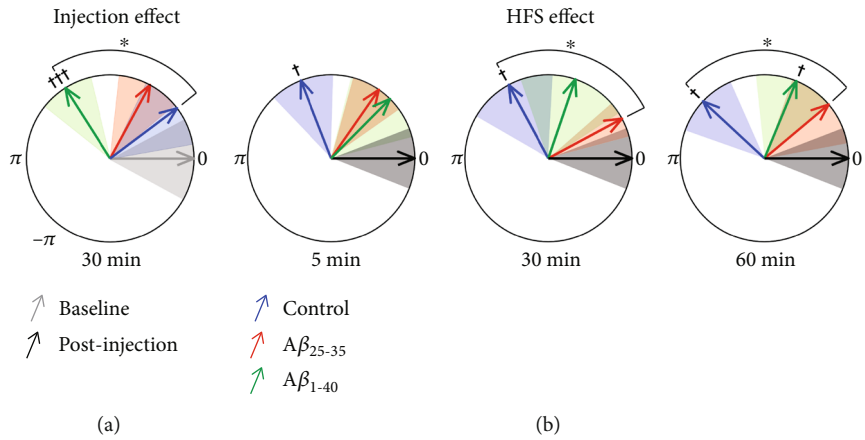

Figure 5: Peptide injection and HFS shifted the θ-to-γ PAC average phase vector. (a) Circular diagram illustrating the intrahippocampal microinjection-induced shift of the θ-to-γ PAC average phase vector for each group respecting the baseline vector. (b) Circular diagrams illustrating the time evolution (at 5, 30, and 60 min) of HFS-induced shift of the θ-to-γ PAC average phase vector for each group respecting the microinjection vector. Coloured arrows indicate average vector angles (control, blue; Aβ25-35, red; and Aβ1-40, green); correspondingly coloured shaded areas illustrate the standard error of angles for each group. Significant differences relative to the reference vector ($^{\dagger}p < 0.05$, $^{\dagger\dagger\dagger}p < 0.001$); significant differences between groups ($^{*}p < 0.05$).

3.4. Aβ Injection Shifted θ-γ Phase-Amplitude Coupling but Impaired HFS-Induced Shift. To determine if the γ amplitude was linked to the θ phase at the hippocampus, different approaches can be used to calculate PAC. In this case, we calculated the average high-frequency γ power over the modulating low band in θ individual cycles. This method is especially useful when the modulating band is not constant over the length of the experiment. The power distribution was obtained by averaging the entire band, and this average gives a single value for the modulation between the pairs of frequency bands (γ-θ) (for details, see Figure 2 and Supplementary Materials).

A$\beta_{1\text{-}40}$ injection induced a significant γ amplitude-modulating θ phase shift (~122°; $F_{(1,8)} = 37.220$, $p < 0.001$); neither vehicle ($F_{(1,6)} = 1.59$, $p = 0.254$) nor A$\beta_{25\text{-}35}$ ($F_{(1,9)} = 3.26$, $p = 0.104$) injection induced significant shifts in such modulating phase (Figure 5(a)). Planned intergroup comparisons showed that the A$\beta_{1\text{-}40}$ injection-induced phase shift was significantly greater than vehicle injection-induced ($F_{(1,6)} = 7.71$, $p = 0.03$) and A$\beta_{25\text{-}35}$ injection-induced ($F_{(1,9)} = 4.76$, $p = 0.05$) phase shifts; vehicle and A$\beta_{25\text{-}35}$ injection-induced phase shifts were not significantly different to each other ($F_{(1,7)} = 0.43$, $p = 0.53$).

Taking each group injection-induced phase shift as a reference, it was found that HFS induced a significant phase shift (~112-137°) in vehicle-injected subjects (Figure 5(b), blue arrows; $F_{(3,16)} = 4.47$, $p = 0.002$); this phase shift persisted for up to 1 h after HFS (5 min: $F_{(1,4)} = 9.25$, $p = 0.038$; 30 min: $F_{(1,4)} = 7.07$, $p = 0.05$; and 60 min: $F_{(1,4)} = 13.11$, $p = 0.022$). In A$\beta_{1\text{-}40}$-injected subjects, HFS induced a smaller phase shift (~45-70°) that reached significance only 60 min

later ($F_{(3,16)} = 1.21$, $p = 0.338$; 5 min: $F_{(1,8)} = 0.72$, $p = 0.421$; 30 min: $F_{(1,8)} = 0.82$, $p = 0.392$; and 60 min: $F_{(1,8)} = 5.55$, $p = 0.046$). By contrast, HFS did not induce a significant phase shift in A$\beta_{25\text{-}35}$-injected animals ($F_{(3,16)} = 1.03$, $p = 0.4073$; 5 min: $F_{(1,8)} = 2.75$, $p = 0.136$; 30 min: $F_{(1,8)} = 0.92$, $p = 0.366$; and 60 min: $F_{(1,8)} = 0.25$, $p = 0.631$).

4. Discussion

This experiment's main findings were that, even though intrahippocampal microinjection of soluble species of Aβ did not change basal transmission, it significantly affected several other properties of cCA3-to-CA1 synapses: (1) A$\beta_{1\text{-}40}$ enhanced basal synaptic variability significantly more than other treatments did but impaired HFS-induced variability increase; (2) A$\beta_{25\text{-}35}$ injection significantly increased gamma and HFO1 band relative PSD; (3) both soluble amyloid beta peptides (A$\beta_{25\text{-}35}$ and A$\beta_{1\text{-}40}$) impaired HFS-induced LTP; and (4) A$\beta_{1\text{-}40}$ injection induced a significant γ amplitude-modulating θ phase shift (~122°) but, as A$\beta_{25\text{-}35}$ did, impaired the occurrence of a HFS-induced phase shift.

Aβ peptides have been repeatedly highlighted as crucial AD pathogenetic initiators. Although the underlying mechanism is not yet fully understood, some studies have indicated that Aβ can impair synaptic transmission and plasticity, leading to changes in spine density and, eventually, synaptic pruning [69–71]. We have found that intrahippocampal microinjection of soluble Aβ in anaesthetized rats affected cCA3-CA1 synapse variability and impaired long-term synaptic plasticity. Overall, such results concur with those of other studies, which have shown that high Aβ oligomer concentration interferes with synaptic efficiency and plasticity [61, 62, 72]. There is a mild increase in fEPSP slope variability after intrahippocampal injection of the vehicle. A similar effect has been observed in other types of *in vivo* preparations [73, 74], possibly due to a mechanical and osmotic effect of the saline solution. Another possibility of that change may involve methylene blue; however, the toxic effects of this molecule *in vitro* have been reported at concentrations higher than 100 μM (around ten times our preparation) [75, 76]. Methylene blue might inhibit Aβ oligomerization in a dose-dependent manner (ranging from 0.01 to 445 μM), but that effect is observed only after several days of incubation (4 to 8 days) [77]. We found that injection of A$\beta_{1\text{-}40}$, but not A$\beta_{25\text{-}35}$, induces significant increases in variability in cCA3-to-CA1 synaptic responses without significant changes in fEPSP slope. In agreement with our results, several *in vivo* studies found that the injection of different amyloid species did not affect hippocampal baseline synaptic potential amplitude or slope [60, 74, 78]. Synaptic variability is determined, among many factors, by presynaptic axonal noise, as well as release probability fluctuations [79]. On the one hand, A$\beta_{1\text{-}42}$ has been found to induce spike widening, which would increase synaptic release due to increased calcium influx into presynaptic boutons [80]; A$\beta_{25\text{-}35}$ has also been reported to produce spike broadening, but using doses one order of magnitude higher than the one used in our experiment [81]. On the other hand, A$\beta_{1\text{-}42}$ oligomers depress release probability at CA3-CA1 synapses [82]; moreover, glutamatergic synaptic transmission could be either enhanced or reduced by A$\beta_{1\text{-}40}$, depending on its concentration and the specific pyramidal cell type affected [44]. Such opposing mechanisms could explain the observed A$\beta_{1\text{-}40}$-induced synaptic variability increase, without significant changes in average fEPSP slope. It is plausible that the A$\beta_{25\text{-}35}$ concentration we used was not enough to induce significant changes in synaptic variability (however, it did affect other synaptic and network properties).

Although neither Aβ-intrahippocampal injection nor HFS induced significant CA1 global power spectrum changes (Suppl. Tables 3 and 4), specific frequency band rPSD computation evidenced that injection with A$\beta_{25\text{-}35}$, but not A$\beta_{1\text{-}40}$ nor HFS, induced a significant γ and HFO_1 relative power increase. Transient (about 100 s) increases in γ and θ spectral power have been recorded in freely behaving adult rats' hippocampus immediately after LTP induction [32]. In the present experiment, such early PSD changes in control subjects were not detected given the 5 min window in our PSD analysis algorithm, which was not designed to detect short-lived changes.

Both γ oscillations and ripples (140-200 Hz) in the CA1 hippocampal region depend critically on the fast-spiking activity of parvalbumin- (PV-) expressing basket cells [83]. Aβ oligomers have been shown to directly interact with receptor tyrosine-protein kinase erbB-4, increasing its phosphorylation state [84]; erbB-4 activation increases PV interneuron-dependent oscillatory activity [85]. PV interneurons' increased activity, which has been described during early stages of AD models in association with subtle cognitive deficits [86, 87], seems to represent an initial adaptive response to Aβ oligomer deposition, which is followed later by PV interneuron dysfunction and more severe cognitive deficits [7, 88]. It is plausible that A$\beta_{25\text{-}35}$ has more affinity than A$\beta_{1\text{-}40}$ for erbB-4.

It has been found that γ band (25-120 Hz) activity increases in close association with locomotor behaviour [89, 90], working memory [91], and memory replay [92]. Hippocampal oscillations at frequencies higher than 100 Hz, also known as ripples (140-200 Hz), have been described to have several implications in cognitive processes [93]. In fact, ripples have been associated with learning and memory consolidation in humans and animals [94–97]. The observed soluble Aβ species-induced modifications in γ band and ripple oscillations in neural circuits are, therefore, associated with synaptic dysfunction and cognitive impairments [47, 98–100].

Both Aβ species used in our experiment (A$\beta_{25\text{-}35}$ and A$\beta_{1\text{-}40}$) impaired HFS-induced LTP in cCA3-to-CA1 synapses. This deleterious effect has been extensively reported, and many possible underlying mechanisms have been identified; among them, those pointing towards excitatory/inhibitory imbalance are relevant to our findings. Aβ-induced calcium dyshomeostasis underlies distorted synaptic transmission, plasticity, and oscillatory activity in the brain. However, depending on exposure time, brain region, oligomer type, and receptor subunits involved, soluble amyloid has been reported not only to inhibit calcium

influx through NMDA receptors in cultured hippocampal [101] or cortical neurons [102] but also to increase NMDA-mediated calcium influx in mouse brains *in vivo* [103]. In addition, deleterious effects of $A\beta_{1\text{-}42}$ and $A\beta_{1\text{-}40}$ on NMDA function and LTP are reverted by a specific GLUN2B receptor antagonist [104]. Acute *in vivo* and *ex vivo* $A\beta_{1\text{-}42}$ administration deteriorates $GABA_B$-mediated inhibitory transmission in CA3-to-CA1 synapses and impairs HFS-induced LTP of excitatory [48] as well as inhibitory potentials [105], and such effects are reverted by pharmacological activation of G-protein-gated inwardly rectifying potassium (GirK) channels. $A\beta_{25\text{-}35}$ has been found to act *ex vivo* as a GirK channel antagonist in CA3 pyramidal neurons [22]. Aβ-induced malfunction of NMDA and GirK channel conductance in pyramidal neurons might contribute, along with PV interneuron dysfunction, to hippocampal network instability, manifested through LTP impairment and aberrant rhythm generation, which may underlie subtle cognitive derailments observed during early AD stages.

Intrahippocampal injection of $A\beta_{1\text{-}40}$ significantly shifted the resulting angle from the average θ-to-γ PAC vector. In vehicle-injected subjects, HFS induced a significant phase shift of the average θ-to-γ PAC vector persisting up to 60 min. Besides impairing HFS-induced LTP, both $A\beta_{25\text{-}35}$ and $A\beta_{1\text{-}40}$ blocked the phase shift of the average θ-to-γ PAC vector, with the $A\beta_{25\text{-}35}$ effect persisting longer. Increases in θ-to-γ coupling have been described in freely behaving rats after HFS-induced LTP; in that experiment, acute $A\beta_{1\text{-}42}$ treatment not only impaired LTP but also diminished θ-to-γ coupling [40]. θ-nested γ oscillations in CA1 depend on out-of-phase firing sequences of PV interneurons, pyramidal cells, somatostatin-positive (SST) neurons, and CA3-activated feedforward inhibitory interneurons during population θ oscillations, eventually opening windows for synaptic plasticity during specific θ phases [106]. Perisomatic inhibition by PV interneurons, associated with temporal silencing of feedforward inhibition acted by SST interneurons, allows calcium spike-associated plasticity; conversely, dendritic inhibition by feedforward interneurons prevents calcium spikes but facilitates pyramidal neuron output [106, 107]. Phase synchronization of firing in such a network depends on the relative contribution of PV (γ band) and SST (θ band) interneurons [108]; therefore, θ-to-γ coupling phase shift represents specific variations in such contributions. The observed Aβ injection-induced phase shift, as well as the impairment of HFS-induced phase shifts, may be due to its effect on PV interneurons [84, 85, 106] and on SST interneurons [108]. There may also be pyramidal cell contribution to such network dysfunction; in fact, $A\beta_{25\text{-}35}$ reduces $GABA_B$-dependent GirK channel activity in pyramidal neurons [22]; this may enhance excitatory pyramidal cell influence on PV and SST interneurons, which would further destabilize the network. Interestingly, in a recent clinical study, restoration of temporal cortex θ-to-γ PAC was associated with working memory performance improvement in older adults [109].

5. Conclusions

The present study results indicate that changes in the functional relationships between θ, γ, and ripple oscillatory network activity in the hippocampus are highly correlated with amyloid-induced synaptic plasticity dysfunction in a model of early amyloid-β pathology (similar to what has been reported in early AD stages). Taken together, these results show that intrahippocampal microinjection of soluble forms of Aβ affects synaptic variability and plasticity and modifies neural processing and network activity, changes that might underlie cognitive deficits observed in early AD models. Aβ-induced derailment of the tight functional relationship in hippocampal circuits between θ oscillation (controlled by SST interneurons as well as by medial septum and entorhinal cortex inputs) and γ activity (controlled by PV interneurons) implies a dysregulation of the crosstalk of cholinergic, glutamatergic, and GABAergic systems during early AD stages, leading to impaired information processing and encoding. Therefore, the abnormality in θ-to-γ PAC hereby described is worth evaluating as a putative early biomarker of Aβ-induced synaptic dysfunction in AD, long before neurodegeneration is established.

AD is a chronic and complex neurological disorder that involves several mechanisms (i.e., neuroinflammation and oxidative stress) additional to amyloid pathology. For that reason, it is important to start considering the role of θ-to-γ PAC in behavioural models of AD that involve tauopathy and selective chronic neurodegeneration, as well as to test it in further clinical trials through noninvasive electrophysiological methods in patients with mild cognitive impairment and major neurocognitive disorder.

Data Availability

Additional data set can be sent by request. Detailed information of methods and results are included in Supplementary Materials.

Disclosure

A preliminary version of this work was presented as a poster in the Joint Meeting of International Brain Research Organization & Federation of Asian-Oceanian Neuroscience Societies.

Conflicts of Interest

The authors declare that they have no conflicts of interest.

Authors' Contributions

Mauricio O. Nava-Mesa and Alejandro Múnera contributed equally to this work.

Acknowledgments

We thank Jeremy Allen, PhD, from Edanz Group (http://www.edanzediting.com/ac) and Tim Hiley for editing a draft of this manuscript. This work was supported by the

Colombian Science and Technology Institute (COLCIENCIAS, project code: 122265840550, CT-160-2015), Universidad del Rosario, and Universidad Nacional de Colombia.

Supplementary Materials

This section includes supplementary methods and supplementary data (Supplementary Tables 1–4). *(Supplementary Materials)*

References

[1] M. Goedert and M. G. Spillantini, "A century of Alzheimer's disease," *Science*, vol. 314, no. 5800, pp. 777–781, 2006.

[2] L. V. Colom, "Septal networks: relevance to theta rhythm, epilepsy and Alzheimer's disease," *Journal of Neurochemistry*, vol. 96, no. 3, pp. 609–623, 2006.

[3] J. J. Palop and L. Mucke, "Network abnormalities and interneuron dysfunction in Alzheimer disease," *Nature Reviews Neuroscience*, vol. 17, no. 12, pp. 777–792, 2016.

[4] R. W. Van Hooren, J. M. Riphagen, H. I. Jacobs, and Alzheimer's Disease Neuroimaging Initiative, "Inter-network connectivity and amyloid-beta linked to cognitive decline in preclinical Alzheimer's disease: a longitudinal cohort study," *Alzheimer's Research & Therapy*, vol. 10, no. 1, p. 88, 2018.

[5] F. C. Quevenco, S. J. Schreiner, M. G. Preti et al., "GABA and glutamate moderate beta-amyloid related functional connectivity in cognitively unimpaired old-aged adults," *NeuroImage: Clinical*, vol. 22, article 101776, 2019.

[6] D. J. Selkoe, "Alzheimer's disease is a synaptic failure," *Science*, vol. 298, no. 5594, pp. 789–791, 2002.

[7] L. Verret, E. O. Mann, G. B. Hang et al., "Inhibitory interneuron deficit links altered network activity and cognitive dysfunction in Alzheimer model," *Cell*, vol. 149, no. 3, pp. 708–721, 2012.

[8] M. O. Nava-Mesa, L. Jiménez-Díaz, J. Yajeya, and J. D. Navarro-Lopez, "GABAergic neurotransmission and new strategies of neuromodulation to compensate synaptic dysfunction in early stages of Alzheimer's disease," *Frontiers in Cellular Neuroscience*, vol. 8, p. 167, 2014.

[9] L.-B. Gao, X.-F. Yu, Q. Chen, and D. Zhou, "Alzheimer's disease therapeutics: current and future therapies," *Minerva Medica*, vol. 107, no. 2, pp. 108–113, 2016.

[10] R. J. Caselli, T. G. Beach, D. S. Knopman, and N. R. Graff-Radford, "Alzheimer disease: scientific breakthroughs and translational challenges," *Presented at the Mayo Clinic Proceedings*, vol. 92, no. 6, pp. 978–994, 2017.

[11] T. Iwatsubo, A. Odaka, N. Suzuki, H. Mizusawa, N. Nukina, and Y. Ihara, "Visualization of Aβ42 (43) and Aβ40 in senile plaques with end-specific Aβ monoclonals: evidence that an initially deposited species is Aβ42 (43)," *Neuron*, vol. 13, no. 1, pp. 45–53, 1994.

[12] A. Güntert, H. Döbeli, and B. Bohrmann, "High sensitivity analysis of amyloid-beta peptide composition in amyloid deposits from human and PS2APP mouse brain," *Neuroscience*, vol. 143, no. 2, pp. 461–475, 2006.

[13] L. Millucci, L. Ghezzi, G. Bernardini, and A. Santucci, "Conformations and biological activities of amyloid beta peptide 25-35," *Current Protein and Peptide Science*, vol. 11, no. 1, pp. 54–67, 2010.

[14] C. J. Pike, A. J. Walencewicz-Wasserman, J. Kosmoski, D. H. Cribbs, C. G. Glabe, and C. W. Cotman, "Structure-activity analyses of beta-amyloid peptides: contributions of the beta 25-35 region to aggregation and neurotoxicity," *Journal of Neurochemistry*, vol. 64, no. 1, pp. 253–265, 1995.

[15] I. Kaneko, K. Morimoto, and T. Kubo, "Drastic neuronal loss in vivo by β-amyloid racemized at Ser 26 residue: conversion of non-toxic [D-Ser 26] β-amyloid 1–40 to toxic and proteinase-resistant fragments," *Neuroscience*, vol. 104, no. 4, pp. 1003–1011, 2001.

[16] M. Gruden, T. Davudova, M. Mališauskas et al., "Autoimmune responses to amyloid structures of A$\beta_{(25-35)}$ peptide and human lysozyme in the serum of patients with progressive Alzheimer's disease," *Dementia and Geriatric Cognitive Disorders*, vol. 18, no. 2, pp. 165–171, 2004.

[17] S. Varadarajan, J. Kanski, M. Aksenova, C. Lauderback, and D. A. Butterfield, "Different mechanisms of oxidative stress and neurotoxicity for Alzheimer's Aβ (1– 42) and Aβ (25–35)," *Journal of the American Chemical Society*, vol. 123, no. 24, pp. 5625–5631, 2001.

[18] A. R. Korotzer, E. R. Whittemore, and C. W. Cotman, "Differential regulation by β-amyloid peptides of intracellular free Ca2+ concentration in cultured rat microglia," *European Journal of Pharmacology: Molecular Pharmacology*, vol. 288, no. 2, pp. 125–130, 1995.

[19] H. Hiruma, T. Katakura, S. Takahashi, T. Ichikawa, and T. Kawakami, "Glutamate and amyloid β-protein rapidly inhibit fast axonal transport in cultured rat hippocampal neurons by different mechanisms," *Journal of Neuroscience*, vol. 23, no. 26, pp. 8967–8977, 2003.

[20] R. Rönicke, A. Klemm, J. Meinhardt, U. H. Schröder, M. Fändrich, and K. G. Reymann, "Aβ mediated diminution of MTT reduction—an artefact of single cell culture?," *PLoS One*, vol. 3, no. 9, article e3236, 2008.

[21] H. Moreno, W. E. Wu, T. Lee et al., "Imaging the Aβ-related neurotoxicity of Alzheimer disease," *Archives of Neurology*, vol. 64, no. 10, pp. 1467–1477, 2007.

[22] M. O. Nava-Mesa, L. Jiménez-Díaz, J. Yajeya, and J. D. Navarro-Lopez, "Amyloid-β induces synaptic dysfunction through G protein-gated inwardly rectifying potassium channels in the fimbria-CA3 hippocampal synapse," *Frontiers in Cellular Neuroscience*, vol. 7, p. 117, 2013.

[23] F. Sotty, M. Danik, F. Manseau, F. Laplante, R. Quirion, and S. Williams, "Distinct electrophysiological properties of glutamatergic, cholinergic and GABAergic rat septohippocampal neurons: novel implications for hippocampal rhythmicity," *The Journal of Physiology*, vol. 551, no. 3, pp. 927–943, 2009.

[24] E. C. Fuchs, A. R. Zivkovic, M. O. Cunningham et al., "Recruitment of parvalbumin-positive interneurons determines hippocampal function and associated behavior," *Neuron*, vol. 53, no. 4, pp. 591–604, 2007.

[25] G. Buzsáki and A. Draguhn, "Neuronal oscillations in cortical networks," *Science*, vol. 304, no. 5679, pp. 1926–1929, 2004.

[26] O. Jensen and L. L. Colgin, "Cross-frequency coupling between neuronal oscillations," *Trends in Cognitive Sciences*, vol. 11, no. 7, pp. 267–269, 2007.

[27] F. P. Battaglia, K. Benchenane, A. Sirota, C. M. Pennartz, and S. I. Wiener, "The hippocampus: hub of brain network communication for memory," *Trends in Cognitive Sciences*, vol. 15, no. 7, pp. 310–318, 2011.

[28] A. Gruart, M. D. Muñoz, and J. M. Delgado-García, "Involvement of the CA3–CA1 synapse in the acquisition of associative learning in behaving mice," *Journal of Neuroscience*, vol. 26, no. 4, pp. 1077–1087, 2006.

[29] A. Gruart and J. M. Delgado-García, "Activity-dependent changes of the hippocampal CA3–CA1 synapse during the acquisition of associative learning in conscious mice," *Genes, Brain and Behavior*, vol. 6, no. s1, pp. 24–31, 2007.

[30] J. M. Muñoz-Cabrera, A. G. Sandoval-Hernández, A. Niño et al., "Bexarotene therapy ameliorates behavioral deficits and induces functional and molecular changes in very-old triple transgenic mice model of Alzheimer´s disease," *PLoS One*, vol. 14, no. 10, article e0223578, 2019.

[31] R. T. Wicks, M. R. Witcher, D. E. Couture et al., "Hippocampal CA1 and CA3 neural recording in the human brain: validation of depth electrode placement through high-resolution imaging and electrophysiology," *Neurosurgical Focus*, vol. 49, no. 1, article E5, 2020.

[32] A. Bikbaev and D. Manahan-Vaughan, "Relationship of hippocampal theta and gamma oscillations to potentiation of synaptic transmission," *Frontiers in Neuroscience*, vol. 2, no. 1, pp. 56–63, 2008.

[33] A. Bikbaev and D. Manahan-Vaughan, "Metabotropic glutamate receptor, mGlu5, regulates hippocampal synaptic plasticity and is required for tetanisation-triggered changes in theta and gamma oscillations," *Neuropharmacology*, vol. 115, pp. 20–29, 2017.

[34] D. Habib, C. K. Tsui, L. G. Rosen, and H. C. Dringenberg, "Occlusion of low-frequency-induced, heterosynaptic long-term potentiation in the rat hippocampus in vivo following spatial training," *Cerebral Cortex*, vol. 24, no. 11, pp. 3090–3096, 2014.

[35] M. J. Jutras, P. Fries, and E. A. Buffalo, "Oscillatory activity in the monkey hippocampus during visual exploration and memory formation," *Proceedings of the National Academy of Sciences of the United States of America*, vol. 110, no. 32, pp. 13144–13149, 2013.

[36] F. Peña-Ortega, "Amyloid beta-protein and neural network dysfunction," *Journal of Neurodegenerative Diseases*, vol. 2013, Article ID 657470, 8 pages, 2013.

[37] V. Nimmrich, A. Draguhn, and N. Axmacher, "Neuronal network oscillations in neurodegenerative diseases," *Neuromolecular Medicine*, vol. 17, no. 3, pp. 270–284, 2015.

[38] J. Wang, Y. Fang, X. Wang, H. Yang, X. Yu, and H. Wang, "Enhanced gamma activity and cross-frequency interaction of resting-state electroencephalographic oscillations in patients with Alzheimer's disease," *Frontiers in Aging Neuroscience*, vol. 9, p. 243, 2017.

[39] R. Goutagny, N. Gu, C. Cavanagh et al., "Alterations in hippocampal network oscillations and theta–gamma coupling arise before Aβ overproduction in a mouse model of Alzheimer's disease," *European Journal of Neuroscience*, vol. 37, no. 12, pp. 1896–1902, 2013.

[40] A. N. Kalweit, H. Yang, J. Colitti-Klausnitzer et al., "Acute intracerebral treatment with amyloid-beta (1–42) alters the profile of neuronal oscillations that accompany LTP induction and results in impaired LTP in freely behaving rats," *Frontiers in Behavioral Neuroscience*, vol. 9, p. 103, 2015.

[41] I. Sánchez-Rodríguez, S. Temprano-Carazo, A. Nájera et al., "Activation of G-protein-gated inwardly rectifying potassium (Kir 3/Gir K) channels rescues hippocampal functions in a mouse model of early amyloid-β pathology," *Scientific Reports*, vol. 7, no. 1, pp. 1–13, 2017.

[42] A. N. Kalweit, B. Amanpour-Gharaei, J. Colitti-Klausnitzer, and D. Manahan-Vaughan, "Changes in neuronal oscillations accompany the loss of hippocampal LTP that occurs in an animal model of psychosis," *Frontiers in Behavioral Neuroscience*, vol. 11, p. 36, 2017.

[43] J. Santos-Torres, A. Fuente, J. M. Criado, A. S. Riolobos, M. Heredia, and J. Yajeya, "Glutamatergic synaptic depression by synthetic amyloid β-peptide in the medial septum," *Journal of Neuroscience Research*, vol. 85, no. 3, pp. 634–648, 2007.

[44] Y. Wang, T. H. Zhou, Z. Zhi, A. Barakat, L. Hlatky, and H. Querfurth, "Multiple effects of β-amyloid on single excitatory synaptic connections in the PFC," *Frontiers in Cellular Neuroscience*, vol. 7, p. 129, 2013.

[45] S. Ashenafi, A. Fuente, J. Criado, A. Riolobos, M. Heredia, and J. Yajeya, "β-Amyloid peptide 25–35 depresses excitatory synaptic transmission in the rat basolateral amygdala 'in vitro," *Neurobiology of Aging*, vol. 26, no. 4, pp. 419–428, 2005.

[46] J. J. Palop and L. Mucke, "Amyloid-β–induced neuronal dysfunction in Alzheimer's disease: from synapses toward neural networks," *Nature Neuroscience*, vol. 13, no. 7, pp. 812–818, 2010.

[47] A. I. Gutiérrez-Lerma, B. Ordaz, and F. Peña-Ortega, "Amyloid beta peptides differentially affect hippocampal theta rhythms in vitro," *International Journal of Peptides*, vol. 2013, Article ID 328140, 11 pages, 2013.

[48] I. Sánchez-Rodríguez, S. Djebari, S. Temprano-Carazo et al., "Hippocampal long-term synaptic depression and memory deficits induced in early amyloidopathy are prevented by enhancing G-protein-gated inwardly-rectifying potassium channel activity," *Journal of Neurochemistry*, vol. 153, no. 3, pp. 362–376, 2020.

[49] C. Kilkenny, W. Browne, I. C. Cuthill, M. Emerson, and D. G. Altman, "Animal research: reporting in vivo experiments: the ARRIVE guidelines," *British Journal of Pharmacology*, vol. 160, no. 7, pp. 1577–1579, 2010.

[50] J. Charan and N. Kantharia, "How to calculate sample size in animal studies?," *Journal of Pharmacology & Pharmacotherapeutics*, vol. 4, no. 4, pp. 303–306, 2013.

[51] K. Hara and R. A. Harris, "The anesthetic mechanism of urethane: the effects on neurotransmitter-gated ion channels," *Anesthesia & Analgesia*, vol. 94, no. 2, pp. 313–318, 2002.

[52] M. P. Sceniak and M. B. Mac Iver, "Cellular actions of urethane on rat visual cortical neurons in vitro," *Journal of Neurophysiology*, vol. 95, no. 6, pp. 3865–3874, 2006.

[53] R. Kramis, C. H. Vanderwolf, and B. H. Bland, "Two types of hippocampal rhythmical slow activity in both the rabbit and the rat: relations to behavior and effects of atropine, diethyl ether, urethane, and pentobarbital," *Experimental Neurology*, vol. 49, no. 1, pp. 58–85, 1975.

[54] G. Paxinos and C. Watson, *A Stereotaxic Atlas of the Rat Brain*, Academic, New York, NY, USA, 1998.

[55] S. Zandieh, R. Hopf, H. Redl, and M. G. Schlag, "The effect of ketamine/xylazine anesthesia on sensory and motor evoked potentials in the rat," *Spinal Cord*, vol. 41, no. 1, pp. 16–22, 2003.

[56] C. Morgan, M. Colombres, M. T. Nuñez, and N. C. Inestrosa, "Structure and function of amyloid in Alzheimer's disease," *Progress in Neurobiology*, vol. 74, no. 6, pp. 323–349, 2004.

[57] L. Millucci, R. Raggiaschi, D. Franceschini, G. Terstappen, and A. Santucci, "Rapid aggregation and assembly in aqueous solution of Aβ (25–35) peptide," *Journal of Biosciences*, vol. 34, no. 2, pp. 293–303, 2009.

[58] F. Peña, B. Ordaz, H. Balleza-Tapia et al., "Beta-amyloid protein (25–35) disrupts hippocampal network activity: role of Fyn-kinase," *Hippocampus*, vol. 20, no. 1, pp. 78–96, 2010.

[59] R. N. Leão, L. V. Colom, L. Borgius, O. Kiehn, and A. Fisahn, "Medial septal dysfunction by Aβ-induced KCNQ channel-block in glutamatergic neurons," *Neurobiology of Aging*, vol. 33, no. 9, pp. 2046–2061, 2012.

[60] A. W. Schmid, M. A. Lynch, and C. E. Herron, "The effects of IL-1 receptor antagonist on beta amyloid mediated depression of LTP in the rat CA1 in vivo," *Hippocampus*, vol. 19, no. 7, pp. 670–676, 2009.

[61] A. V. Goryacheva, S. V. Kruglov, M. G. Pshennikova et al., "Adaptation to intermittent hypoxia restricts nitric oxide overproduction and prevents beta-amyloid toxicity in rat brain," *Nitric Oxide*, vol. 23, no. 4, pp. 289–299, 2010.

[62] S. Hajipour, A. Sarkaki, Y. Farbood, A. Eidi, P. Mortazavi, and Z. Valizadeh, "Effect of gallic acid on dementia type of Alzheimer disease in rats: electrophysiological and histological studies," *Basic and Clinical Neuroscience*, vol. 7, no. 2, pp. 97–106, 2016.

[63] M. Y. Stepanichev, A. Ivanov, N. Lazareva, and N. Gulyaeva, "Neurodegenerative changes induced by injection of ß-amyloid peptide fragment (25-35) in hippocampus are associated with NGF-signalling activation," *Bulletin of Russian State Medical University*, vol. 1, no. 1, 2016.

[64] M. Le Van Quyen and A. Bragin, "Analysis of dynamic brain oscillations: methodological advances," *Trends in Neurosciences*, vol. 30, no. 7, pp. 365–373, 2007.

[65] J. M. Lilly and S. C. Olhede, "Generalized Morse wavelets as a superfamily of analytic wavelets," *IEEE Transactions on Signal Processing*, vol. 60, no. 11, pp. 6036–6041, 2012.

[66] A. B. Tort, R. Komorowski, H. Eichenbaum, and N. Kopell, "Measuring phase-amplitude coupling between neuronal oscillations of different frequencies," *Journal of Neurophysiology*, vol. 104, no. 2, pp. 1195–1210, 2010.

[67] A. Trujillo-Ortiz and R. Hernandez-Walls, *Levene test: Levene's test for homogeneity of variances*, 2003, https://www.mathworks.com/matlabcentral/fileexchange/3375-levenetest MATLAB Central File Exchange.

[68] P. Berens, "Circ Stat: a MATLAB toolbox for circular statistics," *Journal of Statistical Software*, vol. 31, no. 10, pp. 1–21, 2009.

[69] H. Hsieh, J. Boehm, C. Sato et al., "AMPAR removal underlies Aβ-induced synaptic depression and dendritic spine loss," *Neuron*, vol. 52, no. 5, pp. 831–843, 2006.

[70] G. M. Shankar, B. L. Bloodgood, M. Townsend, D. M. Walsh, D. J. Selkoe, and B. L. Sabatini, "Natural oligomers of the Alzheimer amyloid-protein induce reversible synapse loss by modulating an NMDA-type glutamate receptor-dependent signaling pathway," *Journal of Neuroscience*, vol. 27, no. 11, pp. 2866–2875, 2007.

[71] W. Wei, L. N. Nguyen, H. W. Kessels, H. Hagiwara, S. Sisodia, and R. Malinow, "Amyloid beta from axons and dendrites reduces local spine number and plasticity," *Nature Neuroscience*, vol. 13, no. 2, pp. 190–196, 2010.

[72] J. J. Palop and L. Mucke, "Synaptic depression and aberrant excitatory network activity in Alzheimer's disease: two faces of the same coin?," *Neuromolecular Medicine*, vol. 12, no. 1, pp. 48–55, 2010.

[73] K. J. Thompson, M. L. Mata, J. E. Orfila, E. J. Barea-Rodriguez, and J. L. Martinez Jr., "Metabotropic glutamate receptor antagonist AIDA blocks induction of mossy fiber-CA3 LTP in vivo," *Journal of Neurophysiology*, vol. 93, no. 5, pp. 2668–2673, 2005.

[74] A. W. Schmid, D. B. Freir, and C. E. Herron, "Inhibition of LTP in vivo by beta-amyloid peptide in different conformational states," *Brain Research*, vol. 1197, pp. 135–142, 2008.

[75] L. Vutskits, A. Briner, P. Klauser et al., "Adverse effects of methylene blue on the central nervous system," *Anesthesiology*, vol. 108, no. 4, pp. 684–692, 2008.

[76] M. Oz, D. E. Lorke, M. Hasan, and G. A. Petroianu, "Cellular and molecular actions of methylene blue in the nervous system," *Medicinal Research Reviews*, vol. 31, no. 1, pp. 93–117, 2011.

[77] M. Necula, L. Breydo, S. Milton et al., "Methylene blue inhibits amyloid Aβ oligomerization by promoting fibrillization," *Biochemistry*, vol. 46, no. 30, pp. 8850–8860, 2007.

[78] D. B. Freir, D. A. Costello, and C. E. Herron, "Aβ25–35-induced depression of long-term potentiation in area CA1 in vivo and in vitro is attenuated by verapamil," *Journal of Neurophysiology*, vol. 89, no. 6, pp. 3061–3069, 2003.

[79] A. Neishabouri and A. A. Faisal, "Axonal noise as a source of synaptic variability," *PLoS Computational Biology*, vol. 10, no. 5, p. e1003615, 2014.

[80] F. Scala, S. Fusco, C. Ripoli et al., "Intraneuronal Aβ accumulation induces hippocampal neuron hyperexcitability through A-type K+ current inhibition mediated by activation of caspases and GSK-3," *Neurobiology of Aging*, vol. 36, no. 2, pp. 886–900, 2015.

[81] H. Yin, H. Wang, H. Zhang, N. Gao, T. Zhang, and Z. Yang, "Resveratrol attenuates Aβ-induced early hippocampal neuron excitability impairment via recovery of function of potassium channels," *Neurotoxicity Research*, vol. 32, no. 3, pp. 311–324, 2017.

[82] Y. He, M. Wei, Y. Wu et al., "Amyloid β oligomers suppress excitatory transmitter release via presynaptic depletion of phosphatidylinositol-4, 5-bisphosphate," *Nature Communications*, vol. 10, no. 1, pp. 1–18, 2019.

[83] D. Schlingloff, S. Káli, T. F. Freund, N. Hájos, and A. I. Gulyás, "Mechanisms of sharp wave initiation and ripple generation," *Journal of Neuroscience*, vol. 34, no. 34, pp. 11385–11398, 2014.

[84] H. Zhang, L. Zhang, D. Zhou et al., "Ablating ErbB4 in PV neurons attenuates synaptic and cognitive deficits in an animal model of Alzheimer's disease," *Neurobiology of Disease*, vol. 106, pp. 171–180, 2017.

[85] R. H. Andersson, A. Johnston, P. A. Herman et al., "Neuregulin and dopamine modulation of hippocampal gamma oscillations is dependent on dopamine D4 receptors," *Proceedings of the National Academy of Sciences of the United States of America*, vol. 109, no. 32, pp. 13118–13123, 2012.

[86] S. Hijazi, T. S. Heistek, P. Scheltens et al., "Early restoration of parvalbumin interneuron activity prevents memory loss and network hyperexcitability in a mouse model of Alzheimer's disease," *Molecular Psychiatry*, vol. 25, no. 12, pp. 3380–3398, 2020.

[87] J.-O. Hollnagel, S. Elzoheiry, K. Gorgas et al., "Early alterations in hippocampal perisomatic GABAergic synapses

and network oscillations in a mouse model of Alzheimer's disease amyloidosis," *PLoS One*, vol. 14, no. 1, article e0209228, 2019.

[88] E. Verdaguer, S. Brox, D. Petrov et al., "Vulnerability of calbindin, calretinin and parvalbumin in a transgenic/knock-in APPswe/PS1dE9 mouse model of Alzheimer disease together with disruption of hippocampal neurogenesis," *Experimental Gerontology*, vol. 69, pp. 176–188, 2015.

[89] G. Buzsáki and C. H. Vanderwolf, "Cellular bases of hippocampal EEG in the behaving rat," *Brain Research Reviews*, vol. 6, no. 2, pp. 139–171, 1983.

[90] C. Kemere, M. F. Carr, M. P. Karlsson, and L. M. Frank, "Rapid and continuous modulation of hippocampal network state during exploration of new places," *PLoS One*, vol. 8, no. 9, article e73114, 2013.

[91] J. Yamamoto, J. Suh, D. Takeuchi, and S. Tonegawa, "Successful execution of working memory linked to synchronized high-frequency gamma oscillations," *Cell*, vol. 157, no. 4, pp. 845–857, 2014.

[92] M. F. Carr, M. P. Karlsson, and L. M. Frank, "Transient slow gamma synchrony underlies hippocampal memory replay," *Neuron*, vol. 75, no. 4, pp. 700–713, 2012.

[93] M. T. Kucewicz, J. Cimbalnik, J. Y. Matsumoto et al., "High frequency oscillations are associated with cognitive processing in human recognition memory," *Brain*, vol. 137, no. 8, pp. 2231–2244, 2014.

[94] N. Axmacher, C. E. Elger, and J. Fell, "Ripples in the medial temporal lobe are relevant for human memory consolidation," *Brain*, vol. 131, no. 7, pp. 1806–1817, 2008.

[95] G. Girardeau, K. Benchenane, S. I. Wiener, G. Buzsáki, and M. B. Zugaro, "Selective suppression of hippocampal ripples impairs spatial memory," *Nature Neuroscience*, vol. 12, no. 10, pp. 1222-1223, 2009.

[96] W. Ramadan, O. Eschenko, and S. J. Sara, "Hippocampal sharp wave/ripples during sleep for consolidation of associative memory," *PLoS One*, vol. 4, no. 8, article e6697, 2009.

[97] G. Girardeau and M. Zugaro, "Hippocampal ripples and memory consolidation," *Current Opinion in Neurobiology*, vol. 21, no. 3, pp. 452–459, 2011.

[98] J. E. Driver, C. Racca, M. O. Cunningham et al., "Impairment of hippocampal gamma (γ)-frequency oscillations in vitro in mice overexpressing human amyloid precursor protein (APP)," *European Journal of Neuroscience*, vol. 26, no. 5, pp. 1280–1288, 2007.

[99] V. Villette, F. Poindessous-Jazat, A. Simon et al., "Decreased rhythmic GABAergic septal activity and memory-associated oscillations after hippocampal amyloid-pathology in the rat," *Journal of Neuroscience*, vol. 30, no. 33, pp. 10991–11003, 2010.

[100] F. Peña-Ortega and R. Bernal-Pedraza, "Amyloid beta peptide slows down sensory-induced hippocampal oscillations," *International Journal of Peptides*, vol. 2012, Article ID 236289, 8 pages, 2012.

[101] D. Gavello, C. Calorio, C. Franchino et al., "Early alterations of hippocampal neuronal firing induced by Abeta 42," *Cerebral Cortex*, vol. 28, no. 2, pp. 433–446, 2018.

[102] I. Ferreira, L. Bajouco, S. Mota, Y. Auberson, C. Oliveira, and A. Rego, "Amyloid beta peptide 1–42 disturbs intracellular calcium homeostasis through activation of GluN2B-containing N-methyl-d-aspartate receptors in cortical cultures," *Cell Calcium*, vol. 51, no. 2, pp. 95–106, 2012.

[103] M. Arbel-Ornath, E. Hudry, J. R. Boivin et al., "Soluble oligomeric amyloid-β induces calcium dyshomeostasis that precedes synapse loss in the living mouse brain," *Molecular Neurodegeneration*, vol. 12, no. 1, pp. 1–14, 2017.

[104] G. Rammes, F. Seeser, K. Mattusch et al., "The NMDA receptor antagonist radiprodil reverses the synaptotoxic effects of different amyloid-beta (Aβ) species on long-term potentiation (LTP)," *Neuropharmacology*, vol. 140, pp. 184–192, 2018.

[105] I. Sánchez-Rodríguez, A. Gruart, J. M. Delgado-García, L. Jiménez-Díaz, and J. D. Navarro-López, "Role of GirK channels in long-term potentiation of synaptic inhibition in an in vivo mouse model of early amyloid-β pathology," *International Journal of Molecular Sciences*, vol. 20, no. 5, article 1168, 2019.

[106] K. Park, J. Lee, H. J. Jang, B. A. Richards, M. M. Kohl, and J. Kwag, "Optogenetic activation of parvalbumin and somatostatin interneurons selectively restores theta-nested gamma oscillations and oscillation-induced spike timing-dependent long-term potentiation impaired by amyloid β oligomers," *BMC Biology*, vol. 18, no. 1, p. 7, 2020.

[107] B. P. Graham and E. Spera, "On phasic inhibition during hippocampal theta," *Network: Computation in Neural Systems*, vol. 25, no. 1–2, pp. 3–19, 2014.

[108] H. Chung, K. Park, H. J. Jang, M. M. Kohl, and J. Kwag, "Dissociation of somatostatin and parvalbumin interneurons circuit dysfunctions underlying hippocampal theta and gamma oscillations impaired by amyloid β oligomers in vivo," *Brain Structure and Function*, vol. 225, no. 3, pp. 935–954, 2020.

[109] R. M. Reinhart and J. A. Nguyen, "Working memory revived in older adults by synchronizing rhythmic brain circuits," *Nature Neuroscience*, vol. 22, no. 5, pp. 820–827, 2019.